NANO LETTERS

Letter

pubs.acs.org/NanoLett

# Silicon Nanowire-Induced Maturation of Cardiomyocytes Derived from Human Induced Pluripotent Stem Cells

Yu Tan,[†] Dylan Richards,[†] Ruoyu Xu,[‡] Skylar Stewart-Clark,[†] Santhosh Kumar Mani,[§] Thomas Keith Borg,[†,∥] Donald R. Menick,[§] Bozhi Tian,[‡] and Ying Mei*[,†,∥]

[†]Bioengineering Department, Clemson University, Clemson, South Carolina 29634, United States

[‡]Department of Chemistry, the James Franck Institute and the Institute for Biophysical Dynamics, University of Chicago, Chicago, Illinois 60637, United States

[§]Division of Cardiology, Department of Medicine, Gazes Cardiac Research Institute, Medical University of South Carolina, Charleston, South Carolina 29425, United States

[∥]Department of Regenerative Medicine and Cell Biology, Medical University of South Carolina, Charleston, South Carolina 29425, United States

*S* *Supporting Information*

**ABSTRACT:** The current inability to derive mature cardiomyocytes from human pluripotent stem cells has been the limiting step for transitioning this powerful technology into clinical therapies. To address this, scaffold-based tissue engineering approaches have been utilized to mimic heart development in vitro and promote maturation of cardiomyocytes derived from human pluripotent stem cells. While scaffolds can provide 3D microenvironments, current scaffolds lack the matched physical/chemical/biological properties of native extracellular environments. On the other hand, scaffold-free, 3D cardiac spheroids (i.e., spherical-shaped microtissues) prepared by seeding cardiomyocytes into agarose microwells were shown to improve cardiac functions. However, cardiomyocytes within the spheroids could not assemble in a controlled manner and led to compromised, unsynchronized contractions. Here, we show, for the first time, that incorporation of a trace amount (i.e., ~0.004% w/v) of electrically conductive silicon nanowires (e-SiNWs) in otherwise scaffold-free cardiac spheroids can form an electrically conductive network, leading to synchronized and significantly enhanced contraction (i.e., >55% increase in average contraction amplitude), resulting in significantly more advanced cellular structural and contractile maturation.

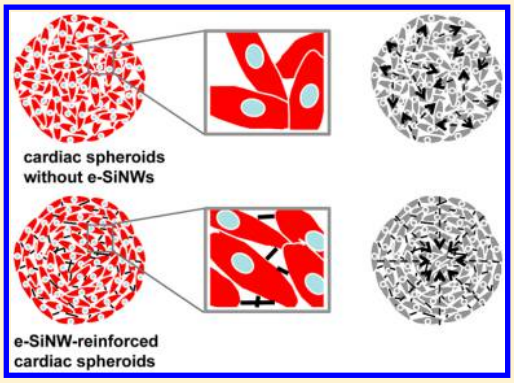


**KEYWORDS:** *silicon nanowires, cardiac spheroids, cardiomyocytes, human induced pluripotent stem cells, maturation*

Cardiovascular disease is the leading cause of death worldwide.[1] Due to the limited regenerative capacity of adult hearts, therapies based on human embryonic stem cells (hESC) and human-induced pluripotent stem cells (hiPSC) have been the focus of a significant amount of research.[2,3] This is due to their proven capacity to produce de novo cardiomyocytes. However, the current cardiomyocytes derived from hESCs and hiPSCs retain an immature phenotype, including poorly organized sarcomere structures (i.e., functional units of the contractile machinery).[4−6] Thus, these cells lack the ability to generate sufficient, anisotropic forces as adult cardiomyocytes. This has led to difficulties for electrical and mechanical integration with human adult myocardium,[7,8] which has limited the applications of hESC and hiPSC technology for cardiac repair.

During embryonic development, environmental factors (e.g., extracellular matrix, growth factors, and mechanical and electrical stimulation) have major effects on the maturation of cardiomyocytes. To mimic the maturation process in vitro, hESC- and hiPSC-derived cardiomyocytes have been mixed with scaffolding materials (e.g., Matrigel and collagen type I gel) to prepare cardiac tissue-engineered constructs and then conditioned with electrical or mechanical stimulation.[4,9−11] Although these scaffolds can provide tissue-like 3D microenvironments, current scaffolding materials lack the matched physical/chemical/biological properties with the native extracellular environments during heart development. On the other hand, scaffold-free, 3D cardiac spheroids have emerged as promising model systems to mimic cardiac tissues.[12,13] Unlike in the myocardium, cardiomyocytes in the spheroids do not organize in a controlled manner and led to compromised, unsynchronized contractions. To improve this, we reasoned the incorporation of electrically conductive silicon nanowires (e-SiNWs) in cardiac spheroids can facilitate the formation of an

**Received:** June 13, 2014
**Revised:** March 9, 2015
**Published:** March 31, 2015





DOI: 10.1021/nl502227a
*Nano Lett.* 2015, 15, 2765−2772

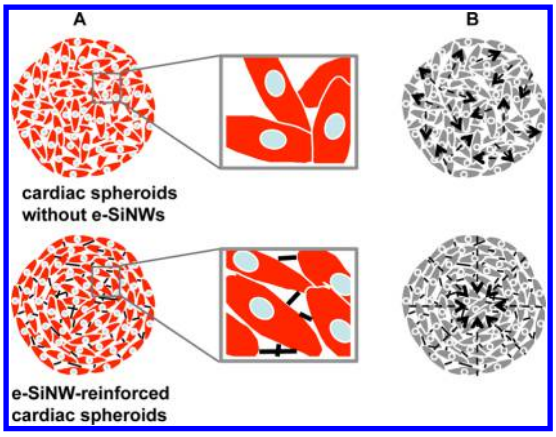


**Figure 1.** Schematic overview of e-SiNWs reinforced cardiac spheroids. (A) Structure of cardiac spheroids without (top) or with (bottom) e-SiNWs: cardiac cells (red), nuclei (blue), and e-SiNWs (black). e-SiNWs (bottom) can act as bridges to electrically connect cardiac cells and create electrically conductive microenvironments throughout the spheroids. (B) Cardiomyocytes in the cardiac spheroids without e-SiNWs (top) form electrically isolated small beating clusters with random contractions, whereas cardiomyocytes in the e-SiNWs reinforced cardiac spheroids can produce synchronized and enhanced contractions (bottom). Arrows represent the directions of contractile forces.

electrically conductive network and provide synchronized and improved electrical/mechanical signals to advance structural and contractile maturation of the cardiomyocytes (Figure 1 and Supporting Information Figure 1).

This approach has the distinct advantage in that only a trace amount of e-SiNWs is utilized, minimizing the adverse effects of traditional scaffolds, such as unmatched physical/chemical/biological properties with the native extracellular environments during heart development. e-SiNWs were selected because of their controllable electrical conductivity, tunable dimensions, and convenient surface tailorability.[14,15] Although SiNWs might not be well known as biocompatible materials, in vitro biocompatibility studies have shown no significant cytotoxic effects for both undoped and n-type SiNWs.[16] Further, the recent research showed SiNWs are biodegradable, and their degradation products are found mainly in the form of $Si(OH)_4$ and are metabolically tolerant in vivo.[17−21] This makes them advantageous over other nonbiodegradable, electrically conductive nanomaterials (e.g., gold nanowires, carbon nanotubes, and nanofibers), especially for potential in vivo applications.

In this study, n-type SiNWs (diameter ≈ 100 nm; length ≈ 10 $\mu$m; silane/phosphane = 500) were prepared according to the previously established protocol[22] (Figure 2A,B). The doping ratio and diameter of the e-SiNWs were chosen to obtain a high conductivity (150−500 $\mu$S/$\mu$m) compared to cell culture medium (~1.75 $\mu$S/$\mu$m) and myocardium (~0.1 $\mu$S/$\mu$m) to create highly electrically conductive microenvironments within spheroids.[23,24] The length of the SiNWs was selected to inhibit cell internalization. As shown in Figure 2C−E, both rat neonatal cardiac cells and human induced pluripotent stem cell-derived cardiomyocytes have been used to prepare e-SiNW-

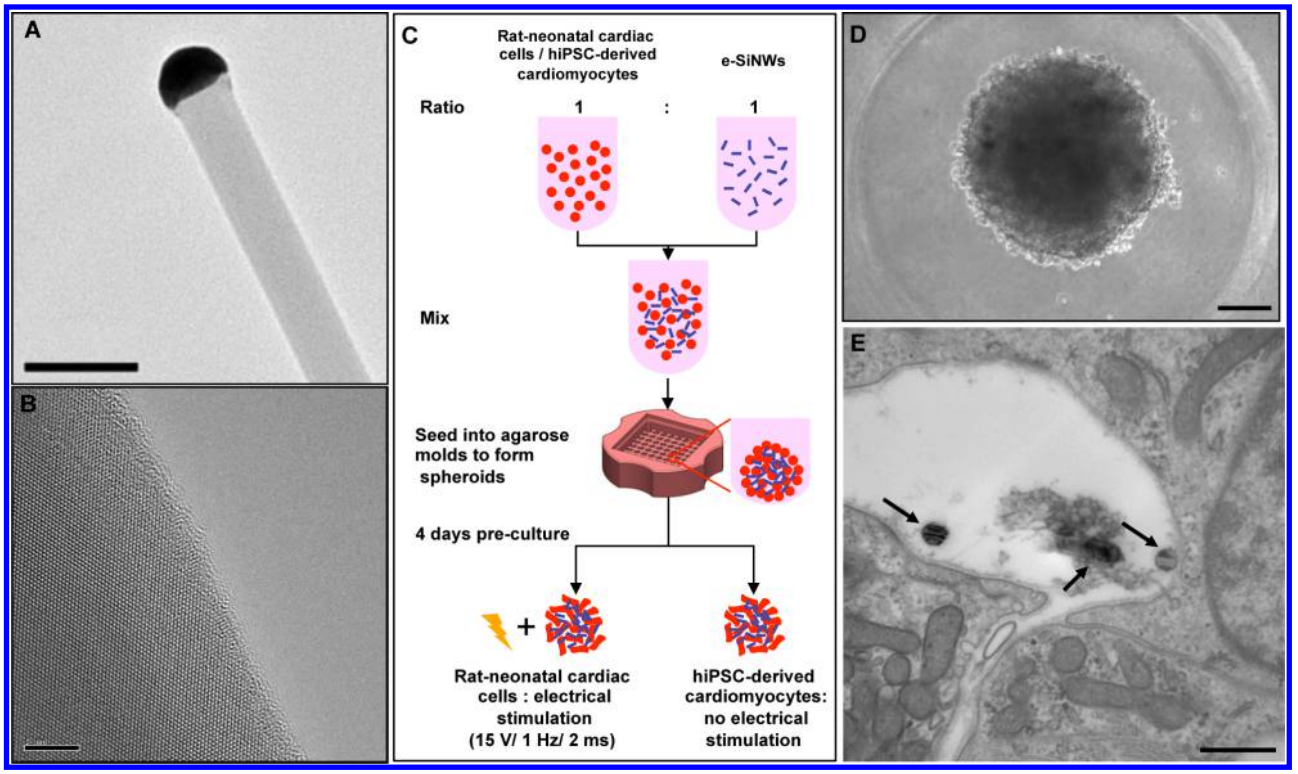


**Figure 2.** Electrically conductive silicon nanowires (e-SiNWs) introduced to cardiac spheroids. (A) Transmission electron microscopy (TEM) image of an e-SiNW (diameter ≈ 100 nm; length ≈ 10 $\mu$m) and (B) high-resolution TEM image of the e-SiNW. (C) Schematic representation of spheroid fabrication using rat-neonatal cardiac cells or human induced pluripotent stem cell (hiPSC)-derived cardiomyocytes at a ratio 1:1 (number of cells/number of e-SiNWs) with or without electrical stimulation. (D) Bright field image of hiPSC spheroid with e-SiNWs. (E) TEM image of hiPSC spheroid with e-SiNWs, black arrow indicates the e-SiNWs located in the extracellular area. Scale bars: (A) 0.2 $\mu$m; (B) 5 nm; (D) 100 $\mu$m; (E) 500 nm.



DOI: 10.1021/nl502227a
*Nano Lett.* 2015, 15, 2765−2772

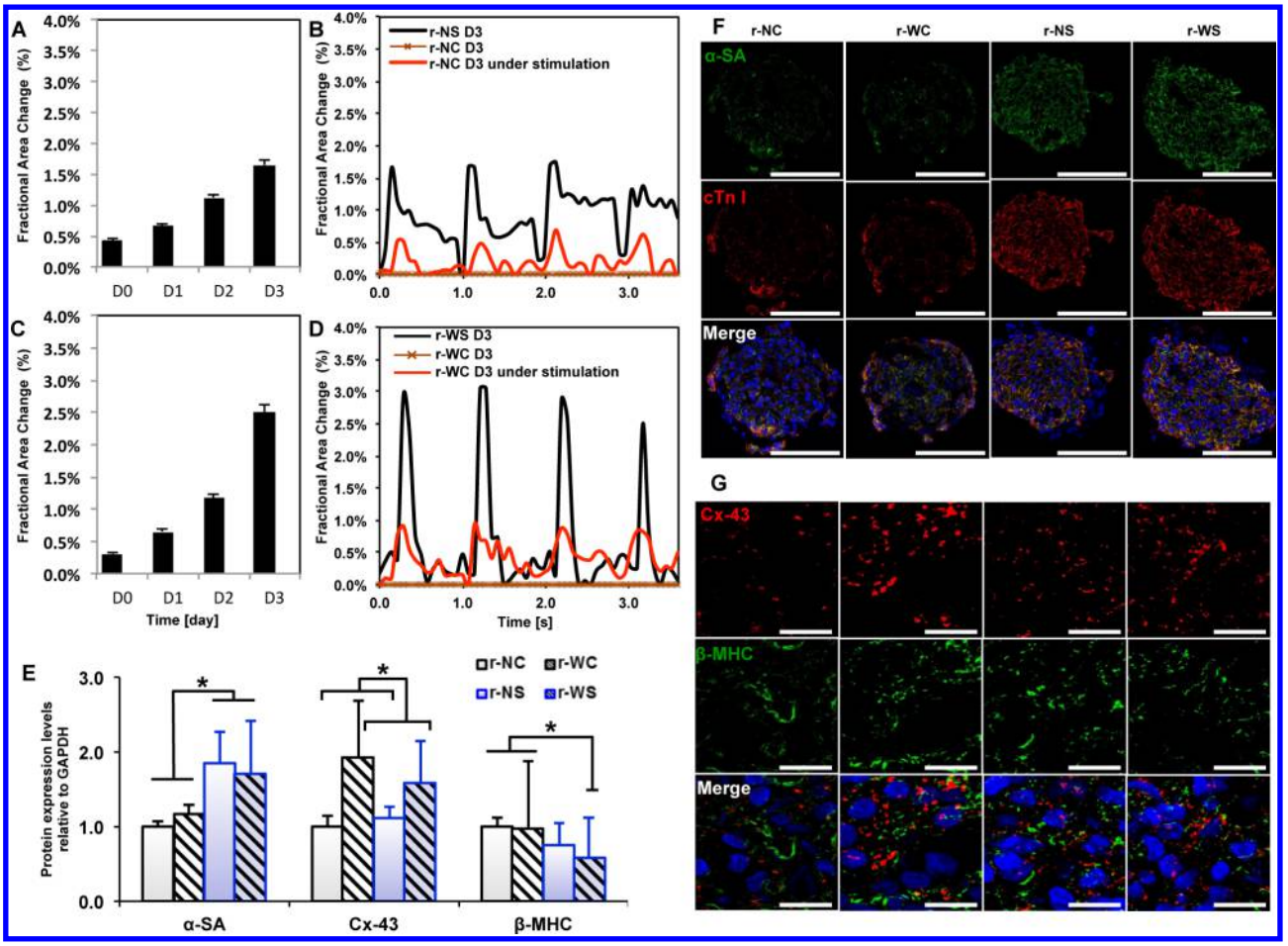


**Figure 3.** Functional and structural analysis of rat-neonatal cardiac spheroids. (A) Averaged fractional area change (i.e., contraction amplitude) over 3 days for r-NS spheroids and (B) a characteristic beating profile on day 3 for r-NC, r-NC under stimulation during measurement, and r-NS spheroids. (C) Averaged fractional area change over 3 days for r-WS spheroids and (D) a characteristic beating profile on day 3 for r-WC, r-WC under stimulation during measurement, and r-WS spheroids. (E) Western blot analysis (averaged data of three separate experiments) of protein expression levels relative to GAPDH expression after 7 days with or without electrical stimulation normalized to the r-NC group. (F, G) Immunofluorescent staining of cardiac-specific contractile and conductive proteins for all groups after 7 days. r-NC = rat-neonatal cardiac spheroids, no e-SiNWs, no stimulation; r-NS = rat-neonatal cardiac spheroids, no e-SiNWs, with stimulation; r-WC = rat-neonatal cardiac spheroids, with e-SiNWs, no stimulation; r-WS = rat-neonatal cardiac spheroids, with e-SiNWs, with stimulation. $n = 6$ spheroids per condition (A–D). Asterisks (*) represent statistical significance with $p < 0.05$; error bars represent standard deviation. Scale bars: (F) 100 $\mu$m; (G) 20 $\mu$m.

reinforced cardiac spheroids. The rat left-ventricle neonatal cardiac cells were utilized in the initial study due to their ready availability. They were mixed with e-SiNWs at a ratio of around 1:1 (number of cells/number of e-SiNWs) and seeded into agarose microwells to prepare e-SiNW-reinforced rat-neonatal cardiac spheroids (Figure 2C,D and Supporting Information Figure 1). The ratio between e-SiNWs and cardiac cells was selected to minimize the interference of e-SiNWs on the self-assembly process of cardiac cells due to their high density and high stiffness (Supporting Information Figure 2). Notably, TEM images of e-SiNW-reinforced cardiac spheroid indicated the e-SiNWs located in the extracellular space in the spheroids, which supported our selection of dimensions of e-SiNWs (Figure 2E).

Although few spontaneous contractions have been found in many rat-neonatal cardiac spheroids after 4 days in culture, both contraction frequency and amplitude can be significantly enhanced by electrical stimulation (Figure 3A–D). To recapitulate the electrical pulses of native myocardium, the spheroids were stimulated at 15 V at 1 Hz, 2 ms.[25] To independently investigate the effects of e-SiNWs and electrical stimulation, four samples have been prepared and examined: rat-neonatal cardiac spheroids without e-SiNWs and without electrical stimulation (i.e., r-NC spheroids), rat-neonatal cardiac spheroids with e-SiNWs but without electrical stimulation (i.e., r-WC spheroids), rat-neonatal cardiac spheroids without e-SiNWs but with electrical stimulation (i.e., r-NS spheroids), and rat-neonatal cardiac spheroids with e-SiNWs and with electrical stimulation (i.e., r-WS spheroids).

Video analysis revealed that the chronically stimulated spheroids (i.e., r-NS and r-WS spheroids) contract regularly and periodically, while the nonstimulated spheroids (i.e., r-NC and r-WC spheroids) did not contract consistently. As shown in Figure 3A–D, the average contraction amplitude gradually increased over time for the chronically stimulated spheroids (i.e., r-NS and r-WS) and was several-fold higher than the nonstimulated spheroids (i.e., r-NC and r-WC) with/without stimulation during measurement, which is consistent with the previous report.[25] When comparing r-NS spheroids with r-WS spheroids, significant improvements in the contraction amplitude and synchronization were found in the r-WS spheroids (Figure 3B, D), which indicates e-SiNWs can


DOI: 10.1021/nl502227a
Nano Lett. 2015, 15, 2765–2772

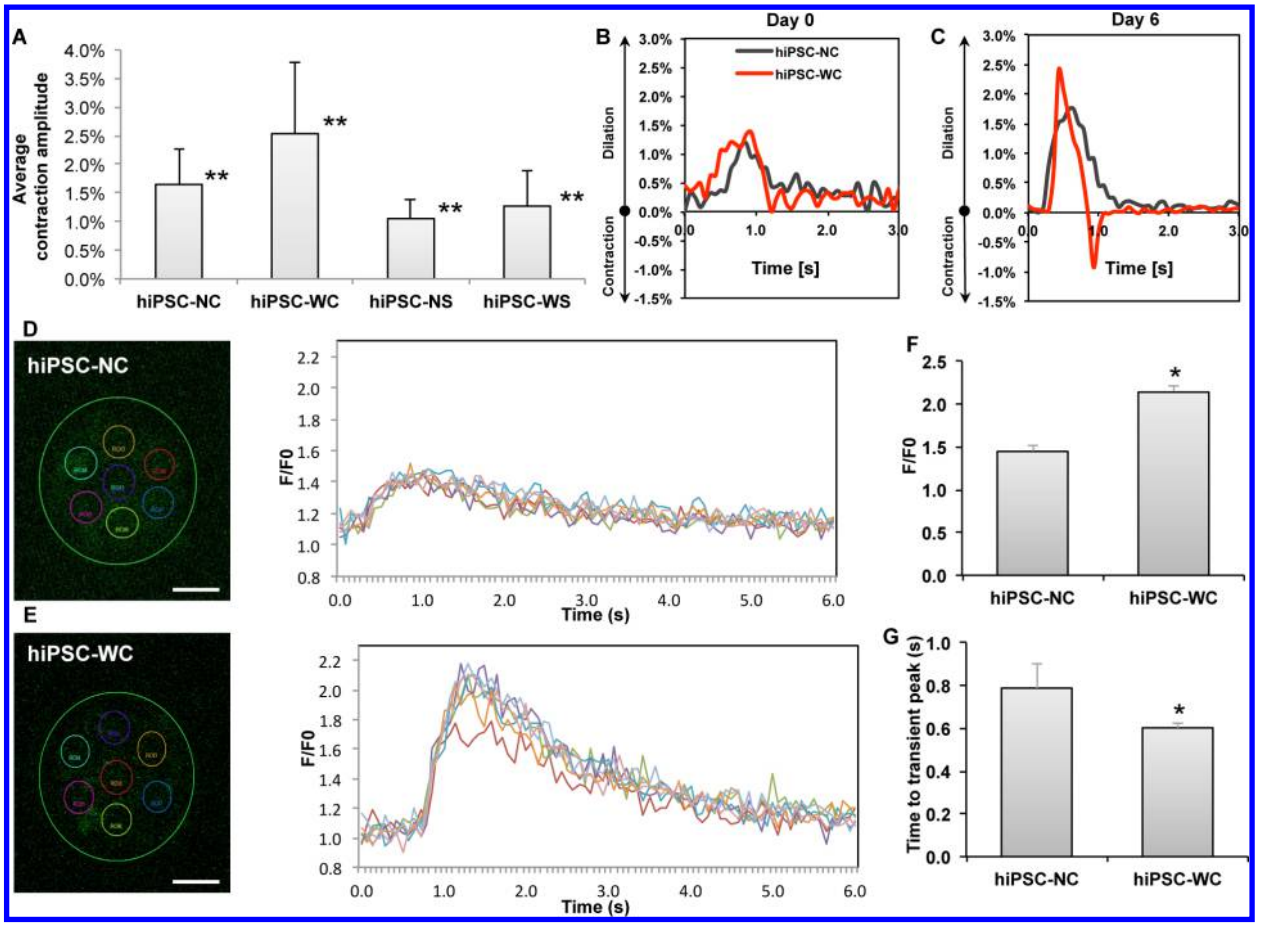


**Figure 4.** Functional analysis of hiPSC-derived cardiomyocyte spheroids. (A) Average contraction amplitude from Day 1 to Day 7 of each group. Double asterisk (**) represents statistical difference between all groups. (B, C) Representative fractional area change (i.e., contraction amplitude) of spontaneously beating spheroids with and without e-SiNWs at time points Day 0 and Day 6; $n = 6$ spheroids per condition. (D, E) Representative calcium transient imaging of seven regions of interest (colored circles) per spheroid for each group. Fluorescence amplitude, $F/F_0$, refers to measured fluorescence intensity normalized to background fluorescence intensity. (F) Comparison of the peak value of $F/F_0$ for each group. ($n = 3$) (G) Comparison of calcium release duration for each group. ($n = 3$) hiPSC-NC = human induced pluripotent stem cell cardiac spheroids, no e-SiNWs, no stimulation; hiPSC-WC = human induced pluripotent stem cell cardiac spheroids, with e-SiNWs, no stimulation. hiPSC-NS = human induced pluripotent stem cell cardiac spheroids, no e-SiNWs, with stimulation; hiPSC-WS = human induced pluripotent stem cell cardiac spheroids, with e-SiNWs, with stimulation. Asterisks (*) represent statistical significance with $p < 0.05$; error bar represents standard deviation. Scale bars = 100 $\mu$m.

facilitate synchronized electrical signal propagation throughout the spheroids.

To understand the effects of e-SiNWs and chronic stimulation, the expressions of several key cardiac-specific proteins in all four different spheroids were examined using Western blotting and immunofluorescence staining (Figure 3E-G and Supporting Information Figure 3A,B). Among them, connexin-43 (i.e., Cx-43) forms gap junction channels that regulate electrical signal propagation between cardiomyocytes.[26,27] Cardiac $\alpha$-sarcomeric actinin ($\alpha$-SA) and cardiac troponin I (cTnI) are cardiac-specific contractile proteins, and $\beta$-myosin heavy chain ($\beta$-MHC) is the neonatal isoform of myosin heavy chain in rat cardiomyocytes.[25] As shown in Figure 3E,F and Supporting Information Figure 3A,B, chronic stimulation can significantly increase the expressions and assembly of contractile proteins (e.g., $\alpha$-SA and cTnI), in agreement with the previous report.[25] On the other hand, the incorporation of e-SiNWs led to enhanced expression and clustering of Cx-43 (Figure 3E,G), also consistent with the previous literature.[28−31] The combination of SiNWs and chronic stimulation can result in the reduced expression of $\beta$-MHC, which indicates a transition from the neonatal isoform of myosin protein to the adult isoform.[25] This could be attributed to the up-regulated Cx-43 expression (Figure 3E,G) or the increased contraction amplitude (Figure 3D).

The results from rat-neonatal cardiac spheroids led to the development of hiPSC cardiac spheroids (i.e., cardiac spheroids prepared from hiPSC-derived cardiomyocytes, Figure 2C). Unlike the rat-neonatal cardiac spheroids, strong spontaneous contractions with consistent contraction frequency were found for the nonstimulated hiPSC cardiac spheroids. Notably, a significant decrease in contraction amplitude was found for electrically stimulated hiPSC-derived cardiac spheroids (i.e., hiPSC-NS and hiPSC-WS spheroids) (Figure 4A). TUNEL staining (marker of early apoptosis) of the spheroid sections revealed significant increase in cell death at the center of hiPSC-NS and hiPSC-WS spheroids, whereas it was not in the r-NS and r-WS spheroids (Supporting Information Figure 4). Given the similar sizes of the rat-neonatal and hiPSC cardiac spheroids, the increased cell death at the center of stimulated hiPSC-derived cardiomyocytes was attributed to the increased metabolic demands of the hiPSC-derived cardiomyocytes compared to rat-neonatal cardiac cells.[32−34] Accordingly, strong expression of the assembled cardiac contractile proteins (e.g., $\alpha$-



DOI: 10.1021/nl502227a
Nano Lett. 2015, 15, 2765−2772

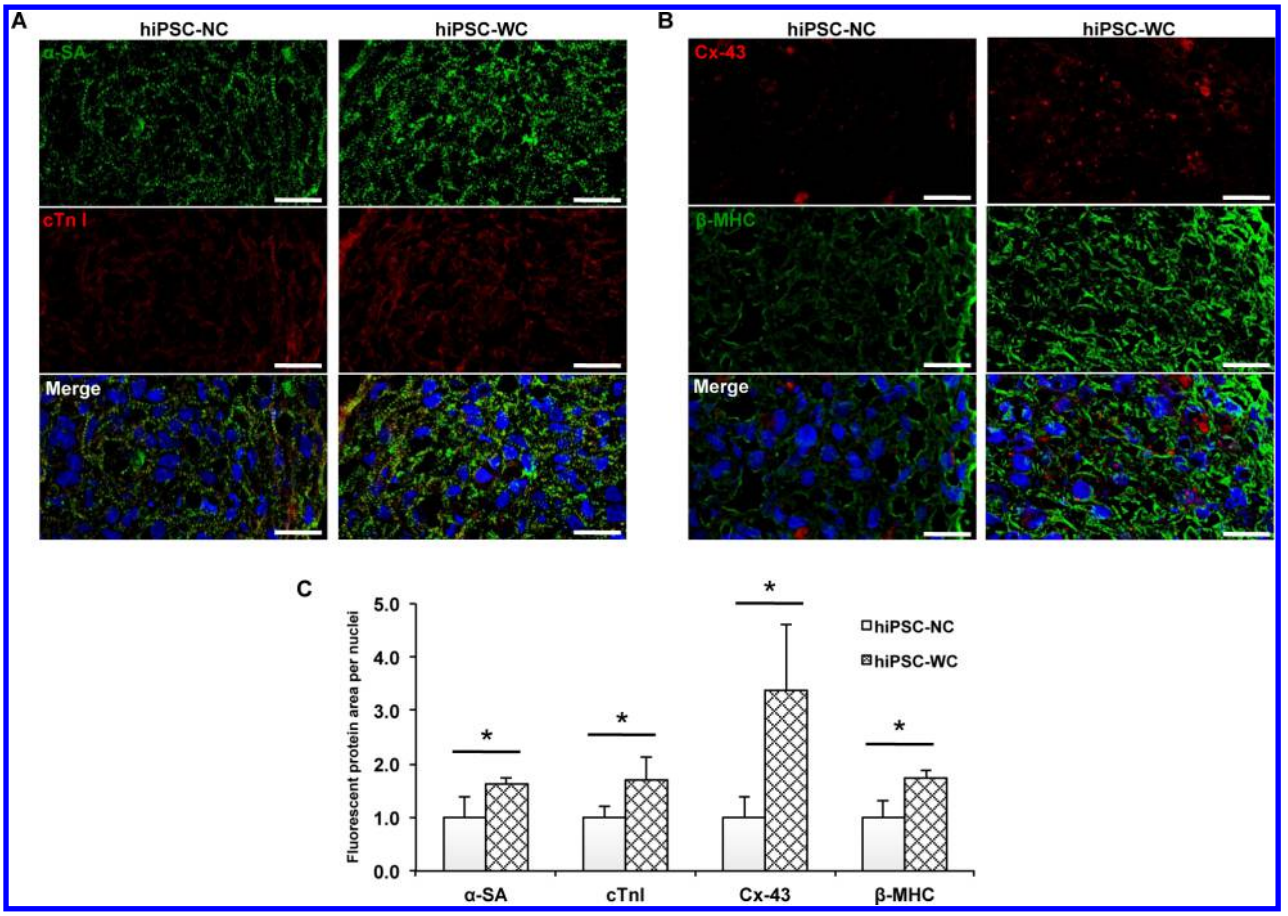


**Figure 5.** Structural analysis of hiPSC-derived cardiomyocyte spheroids. (A) Immunofluorescent staining of alpha sarcomeric actinin ($\alpha$-SA) and troponin I (cTn I). (B) Immunofluorescent staining of connexin-43 (Cx-43) and beta myosin heavy chain ($\beta$-MHC). (C) Protein expression analysis based on fluorescent signal-covered area per nuclei normalized over hiPSCNC expression ($n$ = 3; 75 $\mu$m × 130 $\mu$m picture regions, at least containing >50 nuclei) based on (A, B). hiPSC-NC = human induced pluripotent stem cell cardiac spheroids, no e-SiNWs, no stimulation; hiPSC-WC = human induced pluripotent stem cell cardiac spheroids, with e-SiNWs, no stimulation. Asterisks (*) represent statistical significance with $p < 0.05$; error bar represents standard deviation. Scale bars = 20 $\mu$m.

SA and c-TnI) can only be found on the periphery of the hiPSC-NS and hiPSC-WS spheroids (Supporting Information Figure 5A,B).

On the other hand, the addition of e-SiNWs into hiPSC cardiac spheroids without electrical stimulation (i.e., hiPSC-WC spheroids) can lead to significant improvement in contraction amplitude and synchronization. As shown in Figure 4A, the contraction amplitude of the hiPSC-WC spheroids averaged more than 55% higher than the hiPSC-NC spheroids from Day 1 to Day 7. The sharper peaks of fractional area change of the hiPSC-WC spheroids over the hiPSC-NC spheroids strongly indicated the enhanced contraction synchronization (Figure 4B,C). This is further supported by calcium transient imaging of whole spheroids (Figure 4D,E). The quantification of calcium imaging of spheroids revealed the hiPSC-WC spheroids have an increased overall amplitude ($F/F_0$) of calcium levels and an accelerated time to peak of the calcium transient (Figure 4F,G), which supported the enhanced synchrony during spontaneous contraction. The significant improvement in contraction amplitude and synchronization of hiPSC-WC spheroids is remarkable, considering only a trace amount of e-SiNWs (i.e., 0.004% w/v) was utilized to create e-SiNW-reinforced cardiac spheroids.

The enhanced contraction amplitude and synchronization of the hiPSC-WC spheroids resulted in improved functional maturation. As shown in Figure 5A−C and Supporting Information Figure 5C,D, the immunofluorescence staining indicated the significant increase in expression level and assembly of both conductive and contractile proteins (e.g., Cx-43, $\alpha$-SA, and cTnI) in the hiPSC-WC spheroids, which was further supported by the increased expression of conductive gene GJA1 (Cx-43) and contractile gene MYL2 (ventricle isoform of myosin light chain) (Supporting Information Figure 6). In addition, Figure 4D-G showed the improved peak calcium amplitude and the speed of calcium release, which suggest the improved calcium handling channels and indicates increased maturation. This is further supported by the increased ratio of gene expression of the calcium channel L-type/T-type subunits (CACNA1C/CACNA1G) (Supporting Information Figure 6). The improved calcium handling properties can be attributed to the enhanced organization of the sarcomere structures in the hiPSC-WC spheroids.[35]

To confirm the effects of e-SiNW-reinforced 3D cell culture on the structural and contractile maturation of hiPSC-derived cardiomyocytes, monolayer cells were obtained from hiPSC cardiac spheroids by seeding them onto gelatin-coated substrates, which was thought to minimize dramatic stress usually associated with mechanical/enzymatic spheroid dissociation processes. Sarcomere length and Z-line width were measured as they were known as effective indicators of twitch


DOI: 10.1021/nl502227a
Nano Lett. 2015, 15, 2765−2772

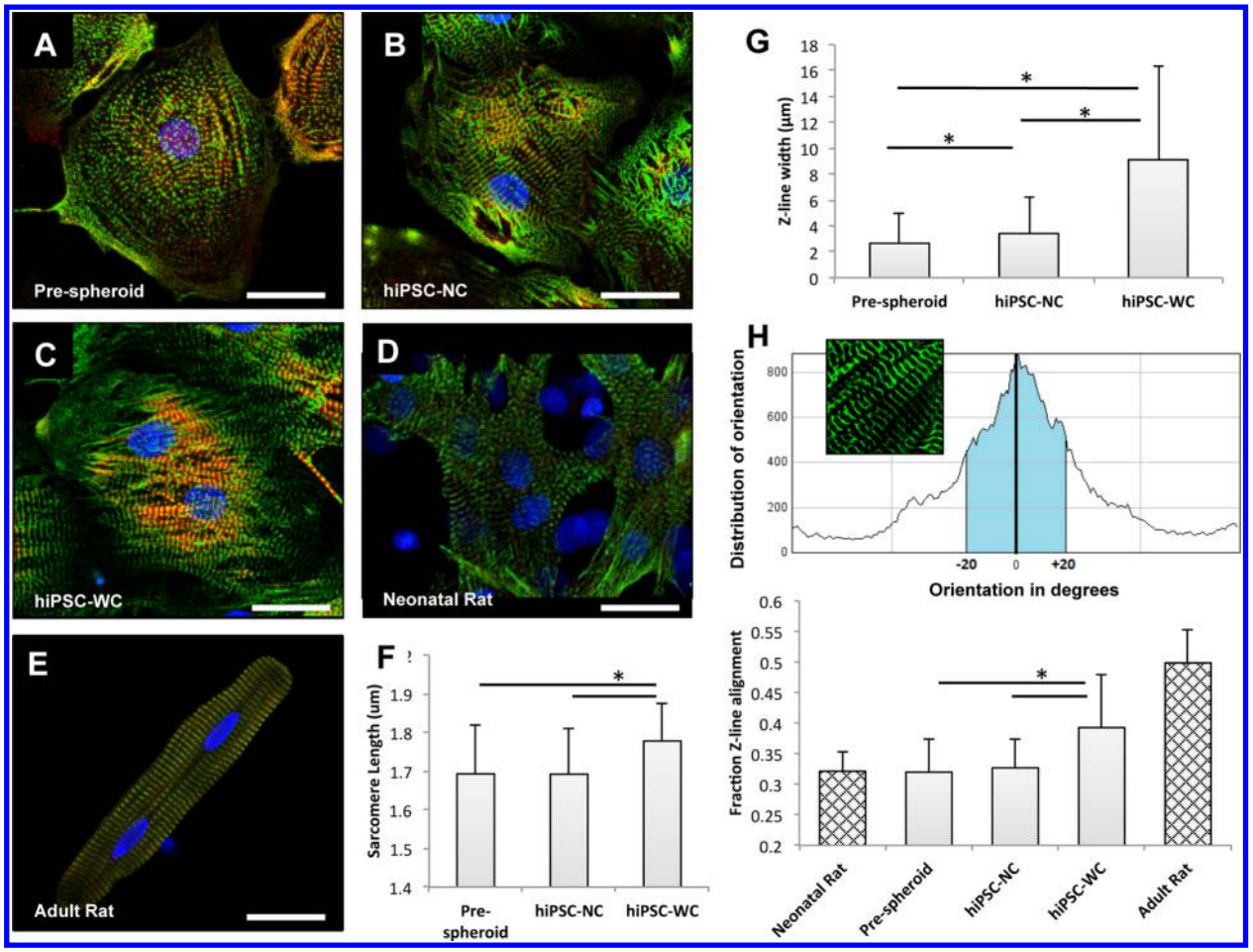


**Figure 6.** Single cell analysis of hiPSC-derived cardiomyocytes before and after spheroids as well as rat-neonatal and adult cardiomyocytes. (A) Fluorescent confocal images (green, $\alpha$-sarcomeric actinin ($\alpha$-SA); red, troponin I; blue, DAPI nuclear stain) of single cells harvested before hiPSC spheroid fabrication, (B) after 7 days from hiPSC-NC spheroids, (C) and after 7 days from hiPSC-WC spheroids. (D) Rat-neonatal cardiomyocyte and (E) adult left ventricular cardiomyocyte for morphological comparison. (F) Sarcomere length measured as distance between $\alpha$-SA-stained Z-line structures from cardiomyocytes with visible sarcomere structures; $n$ = 9 cells per condition. (G) Z-line width measurements based on $\alpha$-SA-stained Z-line structures in comparison to neonatal and adult rat cardiomyocyte references; $n$ = 10 cells per condition. (H) Z-line alignment calculations were based on a fraction ($\pm$20° of the peak orientation degree) of aligned $\alpha$-SA-stained structures; $n$ = 12 cells (hiPSC), 4 cells (rat) per condition. hiPSC-NC = human induced pluripotent stem cell cardiac spheroids, no e-SiNWs, no stimulation; hiPSC-WC = human induced pluripotent stem cell cardiac spheroids, with e-SiNWs, no stimulation. Asterisks (*) represent statistical significance with $p < 0.05$; error bars represent standard deviation. Scale bars = 25 $\mu$m.

force generated by cardiomyocytes[36,37] (Figure 6). As shown in Figure 6A–C and G, cardiomyocytes harvested from both hiPSC-NC and hiPSC-WC spheroids showed significant improvement in Z-line width when compared to prespheroid hiPSC-derived cardiomyocytes. This indicates that 3D culture can provide supportive microenvironments for the maturation of hiPSC-derived cardiomyocytes. Moreover, the hiPSC-WC cardiomyocytes showed significant improvement in both sarcomere length and Z-line width when compared to the hiPSC-NC cardiomyocytes (Figure 6F,G). These improvements were attributed to the enhanced contraction of the hiPSC-WC spheroids. Notably, the alignment of Z-line in hiPSC-WC cardiomyocytes showed remarkable resemblance with adult rat cardiomyocytes (Figure 6C–E and H). The increased sarcomere alignment in the hiPSC-WC spheroids was attributed to the e-SiNW-induced synchronized contractions (Figure 4B,C), which was hypothesized to provide an anisotropic mechanical environment to direct the assembly of contractile machinery of hiPSC-WC cardiomyocytes.

For the first time, we incorporated a trace amount of e-SiNWs into rat-neonatal and hiPSC cardiac spheroids to create electrically conducting microenvironments and induce synchronized and enhanced contraction, which was shown to promote structural and contractile maturation. A long-term culture (i.e., 3 weeks) was conducted to examine whether the addition of e-SiNWs into the hiPSC cardiac spheroids alone is sufficient to derive fully matured hiPSC-derived cardiomyocytes. The improvements in hiPSC-WC spheroids in contraction amplitude, expression level and assembly of contractile protein (e.g., $\alpha$-SA and cTnI) seen at Day 7 were maintained through Day 21 (Supporting Information Figure 7). However, the extended culture did not result in further improvements in the maturation of hiPSC-derived cardiomyocytes. The sarcomere structure and nuclear shape in hiPSC-WC spheroids and hiPSC-NC spheroids at Day 21 resembled that of the Day 7 spheroids (Figure 5, Supporting Information Figures 5 and 7). Our future research will combine additional chemical/physical stimuli (e.g., growth factors, miRNA,


DOI: 10.1021/nl502227a
Nano Lett. 2015, 15, 2765–2772

supporting cells) with e-SiNW-reinforced human cardiac spheroids to produce fully matured hiPSC-cardiomyocytes.[35,38]

Recently, nanocomposite scaffolds composed of electrically conductive nanomaterials and hydrogels have been developed for cardiac tissue engineering applications.[24,29−31] The research reported here is the first demonstration of using nanoscale semiconductors to promote cardiac tissue formation and cardiomyocyte maturation without involving conventional scaffolding materials (e.g., polymers and hydrogels). Also, this research is the first example to directly utilize silicon-based nanomaterials for tissue engineering applications. Our results suggest that silicon-based nanomaterials can have major impacts in tissue engineering. Notably, e-SiNW induced synchronized contraction could have major implications in cell-based cardiac therapy, considering that arrhythmia caused by unsynchronized contraction is a major concern in cardiac surgery.[7,8] Our future research will also include the transplantation of e-SiNW-reinforced hiPSC cardiac spheroids into infarcted hearts to examine their electrical integration with the host myocardium.

## ■ ASSOCIATED CONTENT

### Supporting Information

The experimental details and supplementary figures. This material is available free of charge via the Internet at http://pubs.acs.org.

## ■ AUTHOR INFORMATION


### Corresponding Author

*E-mail: mei@clemson.edu.


### Notes

The authors declare no competing financial interest.

## ■ ACKNOWLEDGMENTS

The work is supported by the National Institutes of Health (8P20 GM103444, U54 GM104941, HL 085847, R01HL095696, R01HL094545), the startup funds from Clemson University, the National Science Foundation (NSF - EPS-0903795), the NIH Cardiovascular Training Grant (T32 HL007260), and a Merit Award from the Veterans' Affairs Health Administration BX002327 to D.R.M. This study used the services of the Morphology, Imaging, and Instrumentation Core, which is supported by NIH-NIGMS P30 GM103342 to the South Carolina COBRE for Developmentally Based Cardiovascular Diseases. We would like to thank Dr. Martin Morad for providing the rat cardiac cells, Dr. Thomas C. Trusk for his technical support in confocal imaging, and Dr. Hongjun Wang and her lab members for the support in Western blotting.

## ■ REFERENCES


(1) Roger, V. L.; Go, A. S.; Lloyd-Jones, D. M.; Adams, R. J.; Berry, J. D.; Brown, T. M.; Carnethon, M. R.; Dai, S.; de Simone, G.; Ford, E. S.; Fox, C. S.; Fullerton, H. J.; Gillespie, C.; Greenlund, K. J.; Hailpern, S. M.; Heit, J. A.; Ho, P. M.; Howard, V. J.; Kissela, B. M.; Kittner, S. J.; Lackland, D. T.; Lichtman, J. H.; Lisabeth, L. D.; Makuc, D. M.; Marcus, G. M.; Marelli, A.; Matchar, D. B.; McDermott, M. M.; Meigs, J. B.; Moy, C. S.; Mozaffarian, D.; Mussolino, M. E.; Nichol, G.; Paynter, N. P.; Rosamond, W. D.; Sorlie, P. D.; Stafford, R. S.; Turan, T. N.; Turner, M. B.; Wong, N. D.; Wylie-Rosett, J. *Circulation* **2011**, *123* (4), e18−e209.

(2) Laflamme, M. A.; Zbinden, S.; Epstein, S. E.; Murry, C. E. *Annu. Rev. Pathol.* **2007**, *2*, 307−39.

(3) Mignone, J. L.; Kreutziger, K. L.; Paige, S. L.; Murry, C. E. *Circ. J.* **2010**, *74* (12), 2517−26.

(4) Nunes, S. S.; Miklas, J. W.; Liu, J.; Aschar-Sobbi, R.; Xiao, Y.; Zhang, B.; Jiang, J.; Masse, S.; Gagliardi, M.; Hsieh, A.; Thavandiran, N.; Laflamme, M. A.; Nanthakumar, K.; Gross, G. J.; Backx, P. H.; Keller, G.; Radisic, M. *Nat. Methods* **2013**, *10* (8), 781−7.

(5) Lundy, S. D.; Zhu, W. Z.; Regnier, M.; Laflamme, M. A. *Stem Cells Dev.* **2013**, *22* (14), 1991−2002.

(6) Lieu, D. K.; Fu, J. D.; Chiamvimonvat, N.; Tung, K. C.; McNerney, G. P.; Huser, T.; Keller, G.; Kong, C. W.; Li, R. A. *Circ.: Arrhythmia Electrophysiol.* **2013**, *6* (1), 191−201.

(7) Shiba, Y.; Fernandes, S.; Zhu, W. Z.; Filice, D.; Muskheli, V.; Kim, J.; Palpant, N. J.; Gantz, J.; Moyes, K. W.; Reinecke, H.; Van Biber, B.; Dardas, T.; Mignone, J. L.; Izawa, A.; Hanna, R.; Viswanathan, M.; Gold, J. D.; Kotlikoff, M. I.; Sarvazyan, N.; Kay, M. W.; Murry, C. E.; Laflamme, M. A. *Nature* **2012**, *489* (7415), 322−5.

(8) Chong, J. J.; Yang, X.; Don, C. W.; Minami, E.; Liu, Y. W.; Weyers, J. J.; Mahoney, W. M.; Van Biber, B.; Palpant, N. J.; Gantz, J. A.; Fugate, J. A.; Muskheli, V.; Gough, G. M.; Vogel, K. W.; Astley, C. A.; Hotchkiss, C. E.; Baldessari, A.; Pabon, L.; Reinecke, H.; Gill, E. A.; Nelson, V.; Kiem, H. P.; Laflamme, M. A.; Murry, C. E. *Nature* **2014**, *510* (7504), 273−277.

(9) Kensah, G.; Roa Lara, A.; Dahlmann, J.; Zweigerdt, R.; Schwanke, K.; Hegermann, J.; Skvorc, D.; Gawol, A.; Azizian, A.; Wagner, S.; Maier, L. S.; Krause, A.; Drager, G.; Ochs, M.; Haverich, A.; Gruh, I.; Martin, U. *Eur. Heart J.* **2013**, *34* (15), 1134−46.

(10) Zhang, D.; Shadrin, I. Y.; Lam, J.; Xian, H. Q.; Snodgrass, H. R.; Bursac, N. *Biomaterials* **2013**, *34* (23), 5813−20.

(11) Mihic, A.; Li, J.; Miyagi, Y.; Gagliardi, M.; Li, S. H.; Zu, J.; Weisel, R. D.; Keller, G.; Li, R. K. *Biomaterials* **2014**, *35* (9), 2798−2808.

(12) Desroches, B. R.; Zhang, P.; Choi, B. R.; King, M. E.; Maldonado, A. E.; Li, W.; Rago, A.; Liu, G.; Nath, N.; Hartmann, K. M.; Yang, B.; Koren, G.; Morgan, J. R.; Mende, U. *Am. J. Physiol.* **2012**, *302* (10), H2031−42.

(13) Kelm, J. M.; Ehler, E.; Nielsen, L. K.; Schlatter, S.; Perriard, J. C.; Fussenegger, M. *Tissue Eng.* **2004**, *10* (1−2), 201−14.

(14) Schmidt, V.; Wittemann, J. V.; Senz, S.; Gosele, U. *Adv. Mater.* **2009**, *21*, 2681−2702.

(15) Tian, B.; Lieber, C. M. *Annu. Rev. Anal. Chem.* **2013**, *6*, 31−51.

(16) Garipcan, B.; Odabas, S.; Demirel, G.; Burger, J.; Nonnenmann, S. S.; Coster, M. T.; Gallo, E. M.; Nabet, B.; Spanier, J. E.; Piskin, E. *Adv. Eng. Mater.* **2011**, *13*, B3−B9.

(17) Jiang, K.; Fan, D.; Belabassi, Y.; Akkaraju, G.; Montchamp, J. L.; Coffer, J. L. *ACS Appl. Mater. Interfaces* **2009**, *1* (2), 266−9.

(18) Nagesha, D. K.; Whitehead, M. A.; Coffer, J. L. *Adv. Mater.* **2005**, *17* (7), 921−924.

(19) Anderson, S. H. C.; Elliott, H.; Wallis, D. J.; Canham, L. T.; Powell, J. J. *Phys. Status Solidi A* **2003**, *197* (2), 331−335.

(20) Zhou, W.; Dai, X.; Fu, T. M.; Xie, C.; Liu, J.; Lieber, C. M. *Nano Lett.* **2014**, *14* (3), 1614−9.

(21) Tolli, M. A.; Ferreira, M. P.; Kinnunen, S. M.; Rysa, J.; Makila, E. M.; Szabo, Z.; Serpi, R. E.; Ohukainen, P. J.; Valimaki, M. J.; Correia, A. M.; Salonen, J. J.; Hirvonen, J. T.; Ruskoaho, H. J.; Santos, H. A. *Biomaterials* **2014**, *35* (29), 8394−405.

(22) Zheng, G. F.; Lu, W.; Jin, S.; Lieber, C. M. *Adv. Mater.* **2004**, *16* (21), 1890−1893.

(23) Mazzoleni, A. P.; Sisken, B. F.; Kahler, R. L. *Bioelectromagnetics* **1986**, *7* (1), 95−9.

(24) Shin, S. R.; Jung, S. M.; Zalabany, M.; Kim, K.; Zorlutuna, P.; Kim, S. B.; Nikkhah, M.; Khabiry, M.; Azize, M.; Kong, J.; Wan, K. T.; Palacios, T.; Dokmeci, M. R.; Bae, H.; Tang, X. S.; Khademhosseini, A. *ACS Nano* **2013**, *7* (3), 2369−80.

(25) Radisic, M.; Park, H.; Shing, H.; Consi, T.; Schoen, F. J.; Langer, R.; Freed, L. E.; Vunjak-Novakovic, G. *Proc. Natl. Acad. Sci. U.S.A.* **2004**, *101* (52), 18129−34.




DOI: 10.1021/nl502227a
*Nano Lett.* 2015, 15, 2765−2772

(26) Beauchamp, P.; Choby, C.; Desplantez, T.; de Peyer, K.; Green, K.; Yamada, K. A.; Weingart, R.; Saffitz, J. E.; Kleber, A. G. *Circ. Res.* **2004**, *95* (2), 170−8.
(27) Beauchamp, P.; Desplantez, T.; McCain, M. L.; Li, W.; Asimaki, A.; Rigoli, G.; Parker, K. K.; Saffitz, J. E.; Kleber, A. G. *Circ. Res.* **2012**, *110* (11), 1445−53.
(28) You, J. O.; Rafat, M.; Ye, G. J.; Auguste, D. T. *Nano Lett.* **2011**, *11* (9), 3643−8.
(29) Dvir, T.; Timko, B. P.; Brigham, M. D.; Naik, S. R.; Karajanagi, S. S.; Levy, O.; Jin, H.; Parker, K. K.; Langer, R.; Kohane, D. S. *Nature Nanotechnol.* **2011**, *6* (11), 720−5.
(30) Martinelli, V.; Cellot, G.; Toma, F. M.; Long, C. S.; Caldwell, J. H.; Zentilin, L.; Giacca, M.; Turco, A.; Prato, M.; Ballerini, L.; Mestroni, L. *ACS Nano* **2013**, *7* (7), 5746−5756.
(31) Zhou, J.; Chen, J.; Sun, H.; Qiu, X.; Mou, Y.; Liu, Z.; Zhao, Y.; Li, X.; Han, Y.; Duan, C.; Tang, R.; Wang, C.; Zhong, W.; Liu, J.; Luo, Y.; Mengqiu Xing, M.; Wang, C. *Sci. Rep.* **2014**, *4*, 3733.
(32) Rana, P.; Anson, B.; Engle, S.; Will, Y. *Toxicol. Sci.* **2012**, *130* (1), 117−31.
(33) Casey, T. M.; Arthur, P. G. *Circulation* **2000**, *102* (25), 3124−9.
(34) Radisic, M.; Malda, J.; Epping, E.; Geng, W.; Langer, R.; Vunjak-Novakovic, G. *Biotechnol. Bioeng.* **2006**, *93* (2), 332−43.
(35) van den Heuvel, N. H.; van Veen, T. A.; Lim, B.; Jonsson, M. K. *J. Mol. Cell. Cardiol.* **2014**, *67*, 12−25.
(36) Rodriguez, A. G.; Han, S. J.; Regnier, M.; Sniadecki, N. J. *Biophys. J.* **2011**, *101* (10), 2455−64.
(37) Bub, G.; Camelliti, P.; Bollensdorff, C.; Stuckey, D. J.; Picton, G.; Burton, R. A.; Clarke, K.; Kohl, P. *Am. J. Physiol.* **2010**, *298* (5), H1616−25.
(38) Yang, X.; Pabon, L.; Murry, C. E. *Circ. Res.* **2014**, *114* (3), 511−23.



DOI: 10.1021/nl502227a
*Nano Lett.* 2015, 15, 2765−2772